Grain boundary electric characterization of Zn 7 Sb 2 O 12 semiconducting ceramic: A negative temperature coefficient thermistor

M. A. L. Nobre and S. Lanfredi

Citation: Journal of Applied Physics **93**, 5576 (2003); doi: 10.1063/1.1566092
View online: http://dx.doi.org/10.1063/1.1566092
View Table of Contents: http://scitation.aip.org/content/aip/journal/jap/93/9?ver=pdfcov
Published by the AIP Publishing

Grain boundary electric characterization of $Zn_7Sb_2O_{12}$ semiconducting ceramic: A negative temperature coefficient thermistor

M. A. L. Nobre[a)]
Faculdade de Ciências e Tecnologia—FCT, Universidade Estadual Paulista—UNESP, CP 467, CEP 19060-900, Presidente Prudente—SP, Brazil

S. Lanfredi[a),b)]
Faculdade de Ciências e Tecnologia—FCT, Universidade Estadual Paulista—UNESP, CP 467, CEP 19060-900, Presidente Prudente—SP, Brazil

(Received 12 September 2002; accepted 16 February 2003)

The electrical properties of the grain boundary region of electroceramic sensor temperature based on inverse spinel $Zn_7Sb_2O_{12}$ were investigated at high temperature. The zinc antimoniate was synthesized by a chemical route based on the modified Pechini method. The electric properties of $Zn_7Sb_2O_{12}$ were investigated by impedance spectroscopy in the frequency range from 5 Hz to 13 MHz and from 250 up to 600 °C. The grain boundary conductivity follows the Arrhenius law, with two linear branches of different slopes. These branches exhibit activation energies with very similar values; the low-temperature ($\leqslant$350 °C) and high-temperature ($\geqslant$400 °C) regions are equal to 1.15 and 1.16 eV, respectively. Dissimilar behavior is observed on the relaxation time (τ) curve as a function of temperature, where a single slope is identified. The negative temperature coefficient parameters and nature of the polarization phenomenon of the grain boundary are discussed. [DOI: 10.1063/1.1566092]

I. INTRODUCTION

Zinc antimoniate ($Zn_7Sb_2O_{12}$) is classified as an inverse-type spinel with a structure similar to $MgAl_2O_4$.[1] In this cubic structure, 2/3 of Zn^{2+} cations are located on the tetrahedral sites, while the remaining 1/3 are located on the octahedral sites. This oxide has received small attention, despite its great potential for application in the advanced materials area, such as ceramic pigment,[2] microstructure controller in ZnO-based varistors,[3] polycrystalline semiconductors[4] and magnetic materials.[5] Currently, the most important set of physical and chemical data on $Zn_7Sb_2O_{12}$ is correlated to ZnO-based varistors, a typical electroceramic device with a highly nonlinear voltage–current characteristic.[6]

A nonlinear relation between voltage and current at low-field applications has been reported for $Zn_7Sb_2O_{12}$ ceramics synthesized via a chemical route.[4] Distinct electrical properties between grain and grain boundary regions have been recently reported for $Zn_7Sb_2O_{12}$ ceramics.[4] This provided further evidence that the grain boundary phenomenon is an intrinsic property in this inverse spinel, when prepared by a chemical route. Another set of nonantimoniate semiconducting ceramics with a spinel structure exhibits thermistor properties with a negative temperature coefficient (NTC),[7] a typical bulk phenomenon. In an earlier report, this property has been described for a $Zn_7Sb_2O_{12}$ ceramic,[8] a promising NTC thermistor synthesized via a modified Pechini method.[4,8]

This article reports on the electrical and relaxational properties of the grain boundary of $Zn_7Sb_2O_{12}$ thermistors investigated by impedance spectroscopy. This ac small-signal analysis technique has been widely used to investigate the electric and dielectric properties, as well as physical and chemical phenomena of several materials.

Materials such as fluorides, fluorophosphates, phosphate,[9] and lithium borate-bismute tungstate glasses,[10] single crystals,[11] and several polycrystalline materials, such as $Na_{0.85}Li_{0.15}NbO_3$ lead-free nonrelaxor ferroelectrics,[12] $Bi_3Zn_2Sb_3O_{14}$,[13] and $Bi_{12}TiO_{20}$ dielectrics[14] have been recently characterized with impedance spectroscopy. When applied to ceramics, this characterization technique allows one to simultaneously analyze both the dielectrical and electrical contributions stemming from grain and grain boundaries. $Zn_7Sb_2O_{12}$ was synthesized using an alternative route of chemical synthesis based on the modified Pechini method.[4,8] A deep insight is presented here for the grain boundary features of the $Zn_7Sb_2O_{12}$ thermistor at high temperatures.

II. EXPERIMENTAL PROCEDURE

A. Synthesis

$Zn_7Sb_2O_{12}$ nanostructured powders were synthesized by a modified polymeric precursor method, a chemical synthesis method based on the route developed by Pechini.[15] This method was modified to allow the use of Sb_2O_3 as a source of antimony cations. The starting reagents for preparing of powders obtained via chemical route were zinc acetate $(CH_3CO_2)_2Zn\cdot 2H_2O$ (99.0% Reagen), citric acid $H_3C_6H_5O_7\cdot H_2O$ (99.5% Reagen), ethylene glycol $HOCH_2CH_2OH$ (98.0% Synth), and antimony oxide Sb_2O_3 (99.0% Riedel). Three moles of citric acid were used for

a)Member of the UNESP/CVMat—Virtual Center of Research in Materials.
b)Author to whom correspondence should be addressed; e-mail: silvania@prudente.unesp.br

each mole of metallic cations to be chelated. A solution containing 60 wt % of citric acid and 40 wt % of ethylene glycol was used. Zinc acetate and citric acid were dissolved in ethylene glycol at 70 °C, while the solution was continuously stirred in a beaker. Considering the low solubility of the zinc acetate in ethylene glycol, a sufficient amount of nitric acid (Merck 65%) was added to the solution for more efficient salt solubilization.

In the sequence, a stoichiometric amount of Sb_2O_3 as well as distilled water and nitric acid in excess were added under constant heating and stirring (90 °C). The complete dissolution of the oxide leads to a colorless and transparent solution. With the complete solubilization of the starting materials, the temperature was raised to 110 °C, promoting the polyester formation. In the beaker, this polymer was calcined in a box furnace at 350 °C for 1 h to attain its partial decomposition, which leads to the formation of a expanded black resin, a brittle material. This material was deagglomerated (350 mesh) in an agate mortar. Further details are presented elsewhere.[16] Crystalline powders were prepared by calcination of the precursor at 900 °C for 1 h. A pellet of $Zn_7Sb_2O_{12}$ was prepared by isostatic pressing at 100 MPa. The sintering via constant heating rate process was carried out in a dilatometer up to 1250 °C (NETZSCH 402, Selb, Germany) at 10 °C/min. A relative density of 97% of the theoretical density (6.00 g/cm^3) was reached.

B. Electrical characterization

Electrical measurements were carried out by impedance spectroscopy on a 8-mm-diameter×2-mm-thick sample. Platinum electrodes were deposited on both faces of the sample by a platinum paste coating (Demetron 308A), which was dried at 800 °C for 30 min. The electrical measurements were taken in the frequency range of 5 Hz to 13 MHz, with an applied potential of 500 mV, using an impedance analyzer controlled by a personal computer. The sample was placed in a sample holder with a two-electrode configuration. The measurements were taken from room temperature to 600 °C with a 50 °C step being the heating rate equal to 1.0 °C/min. A 30-min interval was used prior to the measurement to thermally stabilize the sample. All measurements were performed in air atmosphere. The same measurement procedure and parameters were adopted for data acquisition during the cooling cycle. No type of thermal hysteresis development was identified.

The complex impedance data, $Z^*(\omega)$, were plotted in the complex plane for each temperature. Each point on this curve represents one measurement of $Z''(\omega)$ and $Z'(\omega)$ at a specific angular frequency $\omega(\omega=2\pi f)$. Both components of the impedance were normalized by a geometric factor, A/l, where A represents the electrode area and l the thickness of the sample. This normalization gives raise to the complex resistivity $\rho^*(\omega)$ parameter, according to following relations:

$$\rho^*(\omega)=Z^*(\omega)A/l=[Z'(\omega)+jZ''(\omega)]A/l, \quad (1)$$

where $j=\sqrt{-1}$.

The data were analyzed using the Equivalent Circuit (EQUIVCRT) software program,[17] which analyzes complex immittance spectra. This article focuses exclusively on the grain boundary properties. Some insight on the bulk properties is provided elsewhere.[4,8]

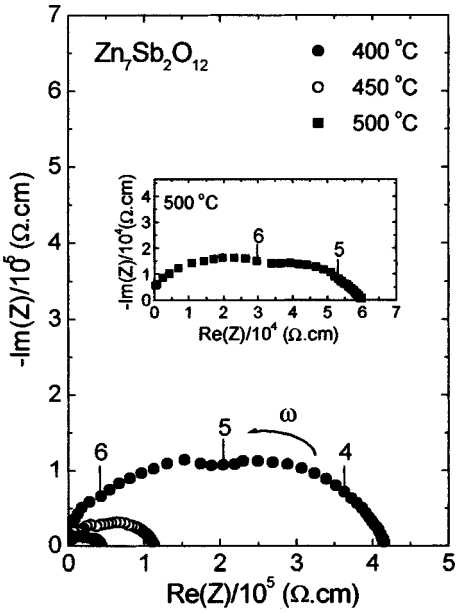

FIG. 1. Impedance diagrams of $Zn_7Sb_2O_{12}$ at several temperatures. Numbers 4, 5, and 6 give the $\log_{10}$ (signal frequency) for the corresponding point.

III. RESULTS AND DISCUSSION

A. Electric resistance analysis

Figure 1 shows impedance diagrams of $Zn_7Sb_2O_{12}$ ceramic obtained at several temperatures. All the semicircles exhibit some depression degree instead of a semicircle centered on the x axis. This decentralization obeys Cole–Cole's formalism. In this formalism, as opposed to the Debye formalism, a depressed semicircle typically represents a phenomenon with a distribution of relaxation times. This nonideal behavior could be correlated to several factors, such as grain orientation, grain boundary, stress-strain phenomena, and atomic defect distribution.

Despite the great number of events that can be correlated to further explain the decentralization phenomenon, this phenomenon has been reported to occur in high-quality single crystals of complex sillenite[14] and in perovskite solid-solution[18] structure, as well as in functional glasses.[9,10] Therefore, this phenomenon is not intercorrelated *a priori* to some kind of quality factor of the material, but is an intrinsic feature of them. The shape of the diagrams suggests that the electrical response is composed of at least two semicircles with similar relaxation frequencies ($f=1/2\pi\tau$).

Figure 2 shows the experimental set of points and a fitted curve for a sample at 400 °C. The points on the diagram are the experimental data, while the continuous line represents the theoretical fit. An excellent agreement between the data and the fitting curve was obtained. The electrical properties of $Zn_7Sb_2O_{12}$ are well represented by two parallel RC equivalent circuits in series. The first contribution

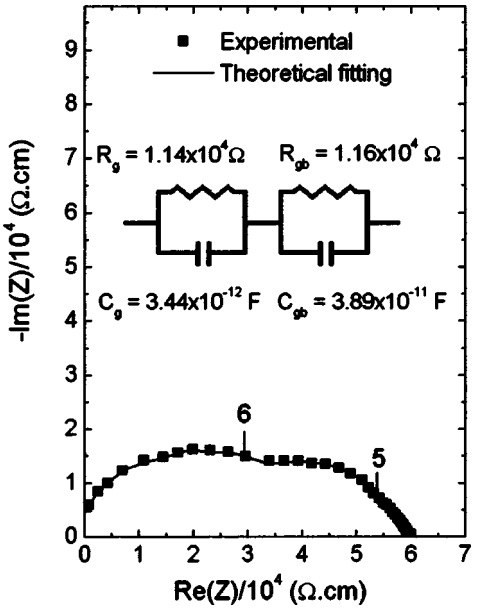

FIG. 2. Experimental data and theoretical fit of $Zn_7Sb_2O_{12}$ with corresponding equivalent circuit obtained at 500 °C. Numbers 4, 5, and 6 give the $\log_{10}$ (signal frequency) for the corresponding point.

($<10^5$ Hz), corresponds to the grain boundary response. The second one, in the high-frequency range ($>10^5$ Hz), corresponds to a bulk response.

Figure 3 shows the grain boundary resistance as a function of temperature. The magnitude of the grain boundary resistance is point-by-point greater than the grain one.[4,8] This is clear evidence that the grain boundary exhibits a higher oxidation state degree than the bulk.[4,8] In Fig. 3, the evolution of the grain boundary resistance values is further characteristic of a NTC thermistor.[8] This behavior has been observed in other thermistor ceramics, being further evidence that the conduction mechanism acting on the grain boundary

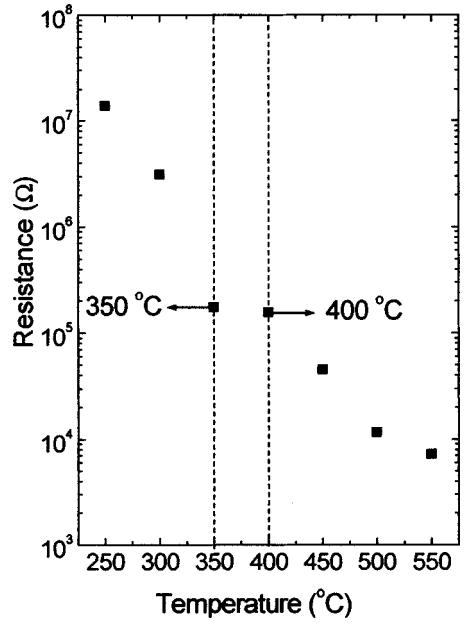

FIG. 3. Grain boundary resistance as a function of temperature.

is of the hopping type,[7] similar to the bulk of $Zn_7Sb_2O_{12}$ reported recently.[8] The curve exhibits two branches at around a specific anomalous region. This anomaly occurs between 350 and 400 °C, at a temperature interval lower than the one reported for bulk $Zn_7Sb_2O_{12}$.[8]

The broadness of the temperature range of the anomaly is relatively small in relation to one typically assigned to the bulk phase transition phenomenon.[8] As a matter of fact, the typical phase transition phenomenon for an inverse spinel is based on the order–disorder-type process,[19] which requires a broad interval of temperature. Thus, based on the temperature range of the anomaly, the phenomenon detected at the grain boundary occurs due a nonstructural event. We speculate that another physicochemical process is responsible for the phenomenon observed, such as an oxireduction of specific species of antimony cations. Unfortunately, the defect chemistry of $Zn_7Sb_2O_{12}$ is almost unknown.

In $Zn_7Sb_2O_{12}$, all antimonium cations occupy octahedral sites and have a state of valence equal to 5+. Nevertheless, the existence of Sb^{3+} cations has been reported[6] for the $Zn_7Sb_2O_{12}$ varistor, a device with properties based on the grain boundary phenomenon.[4] It seems reasonable to assume that the fraction of antimonium cations with valence equal to 3+ should exhibit an almost homogeneous distribution between grain and grain boundary. A slight decrease of concentration of Sb^{3+} at the grain boundary is expected as a function of oxidation phenomenon. Therefore, the Sb^{3+} cation is an intrinsic defect of $Zn_7Sb_2O_{12}$ prepared by the chemical route. For completeness, considering the fundamental electroneutrality role for structural stability, we hypothesize the existence of oxygen vacancies as a second intrinsic defect in this structure. Otherwise, another very realistic approach for the majority defect is to consider the existence of electron holes, a third intrinsic defect of this structure. The existence of electron holes requires further analysis, since this defect is fundamental to development of thermistor properties. At this point, the link between the conduction mechanism expected and experimental data is absent, since the hopping of carriers should occur between cations with valences differing of one unity having in mind that these cations occupy only octahedral sites.[7]

This can be easily solved considering the formation of Sb^{4+} cations[4] in this spinel, which provide the necessary approach to the existence of electron holes. The valence state of 4+ is not unrealistic, when the chemistry of the antimoniate compounds is further considered. Thus, it seems that an oversimplified cation interrelation can be well described by the following equation: $2Sb^{4+} \rightarrow Sb^{3+} + Sb^{5+}$. Furthermore, an intrinsic defect based on the electron hole satisfies the two major requisites to understand the properties of the grain boundary. The first requisite is that oxygen vacancy is not a majority intrinsic defect to the grain boundary. The second one is that the grain boundary exhibits a negative temperature coefficient that is commonly assigned to the electron holes in structures type inverse spinels.

The relation between resistance and temperature for a negative temperature coefficient thermistor is expressed by the following equation:

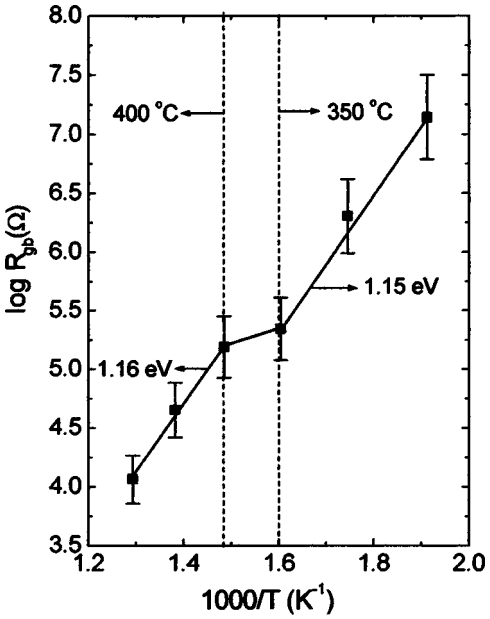

FIG. 4. Arrhenius diagram of the grain boundary resistance of $Zn_7Sb_2O_{12}$.

$$R_T = R_N \exp^{\beta(1/T - 1/T_N)}, \tag{2}$$

where R_T is the resistance at temperature T, R_N is the resistance at known temperature T_N, and β is the thermistor characteristic parameter. Rewriting Eq. (2), β can be derived by the following equation:

$$\beta = [TT_N/(T_N - T)]\ln(R_T/R_N). \tag{3}$$

The thermistor sensitivity is defined by the temperature coefficient of resistance α, which is expressed as a function of parameter β, according to following equation:

$$\alpha = (1/R)[d(R)/dT] = -\beta/T^2. \tag{4}$$

Considering $R-T$ curve (Fig. 3), two β parameters were calculated by Eq. (3). In the first region, in the range from 250 to 350 °C, β is equal to 3828 °C. Above 400 °C, it is equal to 4500 °C.

The α is equal to $-3.12\times10^{-2}\,°C^{-1}$ and $-2.81\times10^{-2}\,°C^{-1}$, at 350 and 400 °C, respectively. Both the parameters β and α derived for the grain boundary do not differ substantially from those of the bulk one.[8] Despite the slight difference in the temperature range considered in the derivation of these values, the bulk exhibits values of β and α equal to 3170 °C and $-2.59\times10^{-2}\,°C^{-1}$, respectively, at temperatures below 350 °C. At temperatures above 400 °C, the bulk exhibits values of β and α equal to 3845 °C and $-1.89\times10^{-2}\,°C^{-1}$, respectively.[8]

The resistance of the grain boundary of $Zn_7Sb_2O_{12}$ follows an Arrhenius law:

$$R_{gb} = R_0 \exp(-E_a/kT), \tag{5}$$

where R_0 represents a pre-exponential factor and E_a, k, and T are, respectively, the activation energy for conduction, Boltzmann's constant, and the absolute temperature.

Figure 4 shows an Arrhenius diagram of grain boundary resistance. As can be seem, the two branches are linear. Nevertheless, despite a good correlation (0.995) attained for each branch, some slight departure of experimental points can be observed. This can be assigned to two factors. The first factor is naturally due to the investigated region involving a physical anomaly. The second one might be due to some kind of synergetic effect between defect chemistry and occupation factor, an intrinsic phenomenon in the inverse-type spinel. $Zn_7Sb_2O_{12}$ ceramic presents very similar values for E_a at low-temperature ($\leqslant$350 °C) and at high-temperature ($\geqslant$400 °C) regions, 1.15 and 1.16 eV, respectively. These values are quite similar, taking into account the existence of two distinct conduction mechanisms. Otherwise, this slight change is compatible with one observed for both the thermistor characteristic parameter (β) and temperature coefficient of resistance (α).

Nevertheless, further analysis should be carefully performed, since the bulk conductivity of this ceramic exhibits two distinct activation energies related to the conduction mechanism.[8] The grain boundary conductivity is smaller than bulk one.[4] It is interesting to note that the ratio between resistance of the grain boundary and grain as a function of temperature is only $\approx$1.0 to 2.5, depending on the temperature. This suggests a decreasing of concentration and/or mobility of carriers due to the enhancement characteristic of the oxidation state of the grain boundary.

B. Electric modulus analysis

Electrical behavior can be investigated via complex electric modulus $M^*(\omega)$ formalism, which provides an alternative approach based on the polarization analysis. However, this formalism takes into account both grain boundary and grain contributions in a coupled way. This one is particularly suitable to detect such phenomena as electrode polarization[20] and such bulk phenomenon properties as apparent conductivity relaxation times τ_σ.[21–23] The electric modulus can be derived by the following equation:

$$M^*(\omega) = j\omega C_0 Z^*(\omega), \tag{6}$$

where C_0 is the vacuum capacitance of the cell.

Figures 5(a) and 5(b) show real part $M'(\omega)$ and normalized-imaginary parts $M''/M''_{\max}$ of the electric modulus as a function of logarithmic frequency for $Zn_7Sb_2O_{12}$ at several temperatures. The electrical polarization is a thermally activated process. According to Fig. 5(a), at all temperatures, $M'(\omega)$ reaches maximum values at a high-frequency region and it tends to zero at low frequencies. Such development suggests a negligible or absent electrode polarization phenomenon. The $M''/M''_{\max}$ parameter exhibits a peak or maximum value with a slight asymmetry at each temperature, as can be seen in Fig. 5(b).

The frequency region below peak frequency f_p determines the range in which charge carriers are mobile over long distances. At the frequency range above f_p, the carriers are confined to potential wells, being mobile over short distances. The peak ($M''_{\max}$) shifts toward higher frequencies with increasing temperature. Above 500 °C, only a part of the curves is obtained due to the uncovered high frequencies.

Figures 6(a) and 6(b) show the variation of normalized parameters tan δ/tan $\delta_{\max}$, $M''/M''_{\max}$, and $Z''/Z''_{\max}$ as a func-

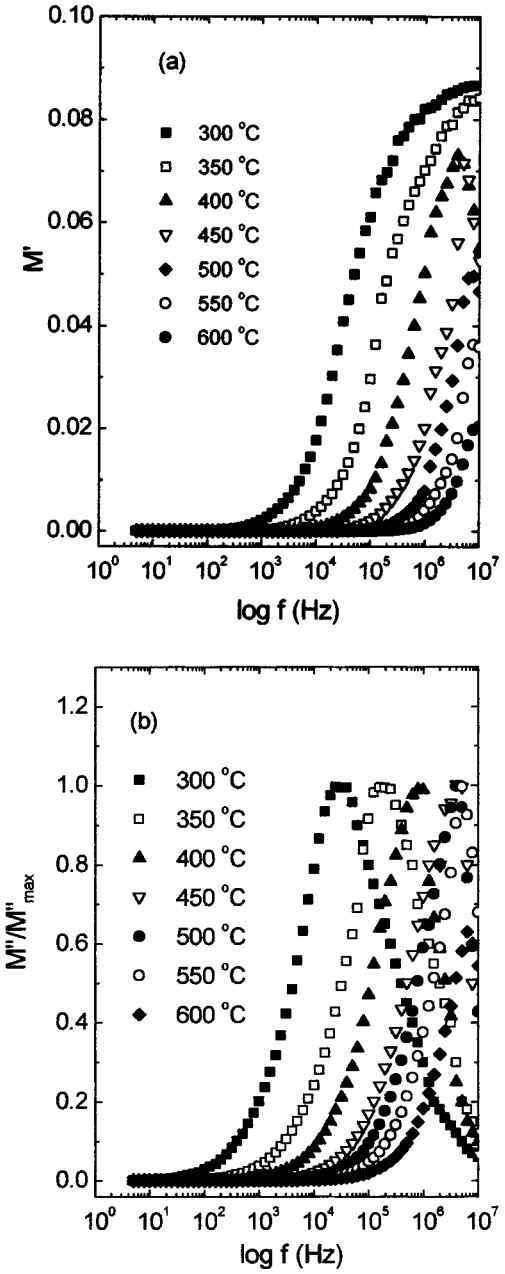

FIG. 5. (a) Real part of the electric modulus (M') and (b) normalized imaginary parts $M''/M''_{\max}$ of the electric modulus as a function of frequency for $Zn_7Sb_2O_{12}$, at several temperatures.

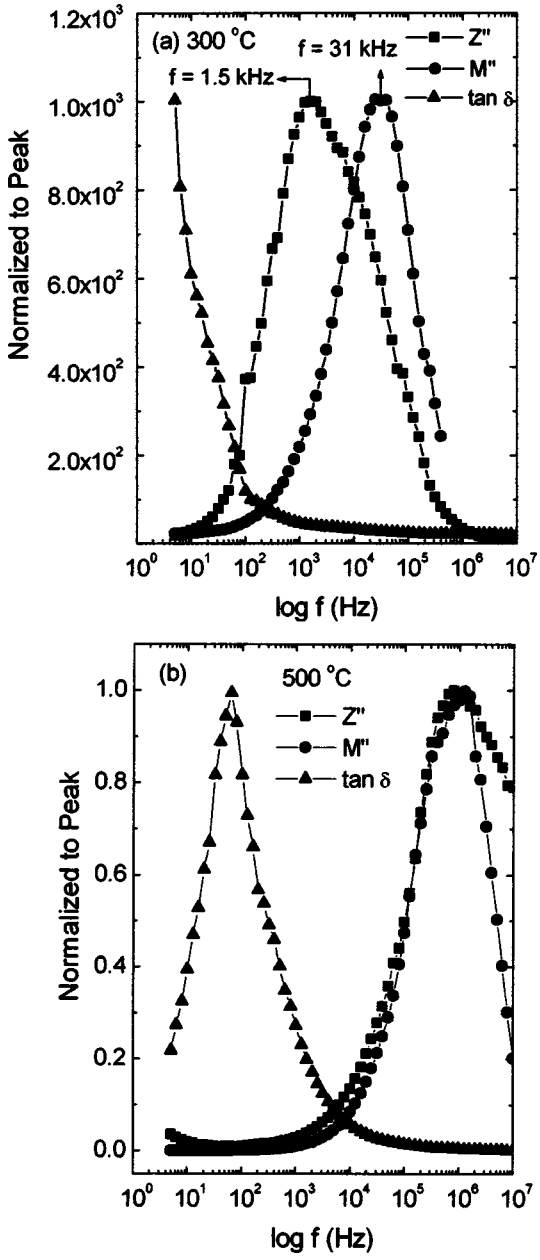

FIG. 6. Normalized tan δ, imaginary part of the impedance (Z'') and imaginary part of the modulus (M'') as a function of frequency for $Zn_7Sb_2O_{12}$ at (a) 300 °C and (b) 500 °C.

tion of logarithmic frequency measured at 300 and 500 °C, respectively. The frequency of the peak in the $M''/M''_{\max}$ curve is slightly shifted to a higher frequency region in relation to the $Z''/Z''_{\max}$ peak. However, the feature of these three functions should be considered simultaneously prior to a precise discerning between localized and nonlocalized conduction. Likewise, the grain boundary contribution should also be examined to distinguish the conduction mechanism. According to Fig. 6(a), the three peaks that describe *a priori* the same relaxation process[24,25] are in complete disaccord with following order proposed elsewhere:[25]

$$\tau_{\tan\delta} > \tau_Z \geqslant \tau_M , \tag{7}$$

where τ is the relaxation time and the subscripts represent the loss tangent ($\tan\delta$) and complex functions $Z^*(\omega)$ and $M^*(\omega)$. The overlapping of peaks of $Z''/Z''_{\max}$ and $M''/M''_{\max}$ ($\tau_Z = \tau_M$) is further evidence of a long-range conductivity.[25] Through these representations, it is possible to observe a change of apparent polarization by inspection of the magnitude of the mismatch between the peaks of both parameters $Z''(\omega)$ and $M''(\omega)$.[24,25] In Fig. 6(a), the presence of an appreciable mismatch between $Z''(\omega)$ and $M''(\omega)$ peaks is further evidence of localized conduction. Therefore, this is in complete accordance with previous discussion, where a hopping conduction is postulated.

However, in Fig. 6(b), the absence of significant mismatch between $Z''(\omega)$ and $M''(\omega)$ peaks suggests a development of delocalized conduction. Furthermore, relation (7) is fully satisfied. In a conventional way, the two characteristic

polarizations ascribed to both grain and grain boundary contributions,[24,25] in accordance with previous discussion, can also induce a slight mismatch between $Z''(\omega)$ and $M''(\omega)$ peaks. However, there is strong evidence to consider a change in the conduction regime from a localized to a delocalized mechanism at high temperatures.

Based on the analysis of Figs. 5(a), 5(b), 6(a), and 6(b), the observed polarization process is due to a localized conduction. It should be pointed that the assignment is unequivocal to the grain or bulk, since the impedance signal is correlated to amount of sample mass. However, the same assignment is nontrivial to the grain boundary, since the amount of mass of the grain boundary is lower than in the grain. Nevertheless, in the subsequent section, a method describing coherent assignment of the polarization type and its mechanism to the grain boundary is presented.

C. Relaxational analysis

The theoretical deconvolution of the electrical response is an effective approach to derive both grain and grain boundary contributions. This can be attained via Boukamp's formalism.[17] In this formalism, the departure from the ideal character of the polarization phenomenon is represented by the Q parameter. In this sense, Q represents a nonideal capacitance[4,8] that is physically determined by the parameters Y_0 and exponent n, where $n \leqslant 1$. Y_0 tends to an ideal capacitance (C) when the exponent n tends to value 1. Thus, the departure from ideal character of the Q is only assigned to a distribution of the relaxation times, which is the physical origin of the decentralization phenomenon. The parameter relaxation time (τ) can be derived of in the conventional way, according to the equation $\tau = RC$.

The temperature dependence of the relaxation time of the grain boundary is represented via a thermally activated process. The logarithmic of grain boundary relaxation time τ_{gb}, as a function of reciprocal temperature $1/T$, is shown in Fig. 7. The derived data are well described by the Arrhenius-type expression:

$$\tau_{gb} = \tau_0 \exp(E_{a\tau}/kT), \tag{8}$$

where τ_0 is the pre-exponential factor or characteristic relaxation time constant and $E_{a\tau}$ is the activation energy for the conduction relaxation. According to Fig. 7, $\log(\tau_{gb})$ decreases linearly with increasing temperature. This means that there is a unique value for $E_{a\tau}$ and τ_0 for the whole range of temperature measurements. It is interesting to note that this temperature range covers the one in which anomalies occur on Figs. 3 and 4, between 350 and 400 °C. This means that the phenomenon observed on Figs. 3 and 4 does not exert a significant influence on the relaxation process. The parameters E_a and τ_0 are equal to 1.10 eV and 2.33×10^{-14} s (i.e., $f_0 = 7.06 \times 10^{12}$ Hz), respectively. Since it is widely known that lattice-related relaxation depends on the defect lattice vibration frequency ($\approx 10^{12}$ Hz), the relaxation process detected for the grain boundary region stems from a lattice defect structure. A reasonable understanding of these phenomena needs further investigation. Currently, the development of a relaxation process based on a simple interfacial polarization phenomenon such as the Maxwell–Wagner mechanism can be discarded. It seems that the relaxation behavior observed for the grain boundary could be ascribed to a space-charge mechanism being an intrinsic feature of grain boundary of $Zn_7Sb_2O_{12}$ thermistor.

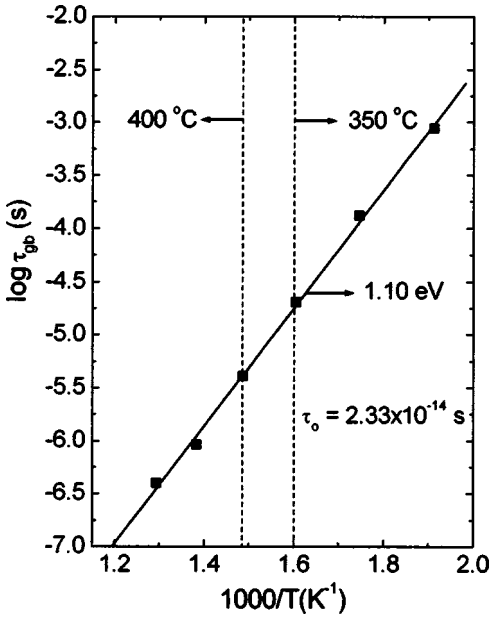

FIG. 7. Arrhenius diagram of grain boundary relaxation time τ_{gb} as a function of reciprocal temperature $1/T$.

Furthermore, the value of activation energy derived is in accord with the one derived from grain boundary electrical resistance, as can be seen in Fig. 4. This means that localized conduction is also active in the grain boundary, similar to the grain.

IV. CONCLUSION

The impedance spectroscopy is a powerful tool to investigate grain boundary phenomena in $Zn_7Sb_2O_{12}$ thermistor ceramics. The grain boundary properties exhibit thermistor parameters at high temperatures with a negative temperature coefficient characteristic, as good as that of the bulk one. The grain boundary exhibits a more stable electrical character in relation to temperature changing due to the high degree of oxidation that leads to a suppression of the phase transition phenomenon observed for the bulk. The grain boundary polarization is due to a space-charge dielectric relaxation mechanism.

ACKNOWLEDGMENTS

This work was supported by the Brazilian research funding institutions FAPESP, CAPES, and CNPq.

[1] K. E. Sickafus, J. M. Wills, and N. W. Grimes, J. Am. Ceram. Soc. **82**, 3279 (2000).
[2] D. Poleti, D. Vasovic, Lj. Karanovic, and Z. Brankovic, J. Solid State Chem. **112**, 39 (1994).
[3] M. A. L. Nobre, M. R. Moraes, E. Longo, and J. A. Varela, *Sintering Science and Technology* (The Pennsylvania State University, State College, 2000), p. 129.
[4] M. A. L. Nobre and S. Lanfredi, Mater. Lett. **50**, 322 (2001).

[5] A. Ilic, B. Antic, D. Rodic, I. Petrovic-Prelevic, and L. J. Karanovic, J. Phys.: Condens. Matter **8**, 2317 (1996).
[6] S. Ezhilvalavan and T. R. Kutty, Appl. Phys. Lett. **68**, 2693 (1996).
[7] J. G. Fagan and V. R. W. Amarakoon, Am. Ceram. Soc. Bull. **72**, 69 (1993).
[8] M. A. L. Nobre and S. Lanfredi, Appl. Phys. Lett. **81**, 451 (2002).
[9] S. Lanfredi, P. S. Saia, R. Lebullenger, and A. C. Hernandes, Solid State Ionics **146**, 329 (2002).
[10] G. S. Murugan and K. B. R. Varma, Solid State Ionics **139**, 105 (2001).
[11] S. Lanfredi, J. F. Carvalho, and A. C. Hernandes, Appl. Phys. Lett. **77**, 4371 (2000).
[12] M. A. L. Nobre and S. Lanfredi, J. Phys.: Condens. Matter **12**, 7833 (2000).
[13] M. A. L. Nobre and S. Lanfredi, Mater. Lett. **47**, 362 (2001).
[14] S. Lanfredi, J. F. Carvalho, and A. C. Hernandes, J. Appl. Phys. **88**, 283 (2000).
[15] M. P. Pechini, U.S. Patent No. 3,330,697 (July 11, 1967).
[16] M. A. L. Nobre, E. Longo, E. R. Leite, and J. A. Varela, Mater. Lett. **28**, 215 (1996).
[17] B. A. Boukamp, *Equivalent Circuit-EQUIVCRT Program—Users Manual* (University of Twente, The Netherlands, 1989), Vol. 3, p. 97.
[18] A. R. James, S. Priya, K. Uchino, and K. Srinivas, J. Appl. Phys. **90**, 3504 (2001).
[19] C. Haas, J. Phys. Chem. Solids **26**, 1225 (1965).
[20] D. P. Almond and A. R. West, Solid State Ionics **11**, 57 (1983).
[21] J. M. Réaux, Xu. Y. J. J. Senegas, Ch. Le Deit, and M. Poulain, Solid State Ionics **95**, 191 (1997).
[22] D. C. Sinclair and A. R. West, J. Appl. Phys. **66**, 3850 (1989).
[23] I. M. Hodge, M. D. Ingram, and A. R. West, J. Electroanal. Chem. **74**, 125 (1976).
[24] W. Cao and R. Gerhardt, Solid State Ionics **42**, 213 (1990).
[25] R. Gerhardt, J. Phys. Chem. Solids **55**, 1491 (1994).